Catalysis Letters
https://doi.org/10.1007/s10562-020-03465-9

Ultrafine and Highly Dispersed Pd/SiO_2 for Suzuki–Miyaura Cross-coupling Reactions

Xizheng Fan[1] · Jingyi Yang[1] · Qingqing Pang[1] · Zhongyi Liu[1] · Panke Zhang[1] · Jing-He Yang[1,2]

Received: 20 September 2020 / Accepted: 12 November 2020

Abstract

Construction of heterogeneous Pd/SiO_2 catalyst via the pollution-free strategy marked strong electrostatic adsorption has been reported for the application to Suzuki–Miyaura cross-coupling reactions. The exposed negatively charged oxygen groups, which were converted from the hydroxyl groups on the surface of silica under the alkaline atmosphere, could effectively anchor palladium species to form ultrafine Pd nanoparticles (Pd NPs) with an average particle size of 1.3 nm and high dispersion (43%). Pd/SiO_2 catalyst was endowed with the excellent catalytic performance which was that the yield of the Suzuki–Miyaura reaction between bromobenzene and phenylboronic acid at 40 °C was > 99% for 30 min and the TOF was ~ 80,000 h^{-1}. The catalyst could be easily recovered and recycled by facile procedure without a significant decrease in catalytic activity, which was able to maintain the 90% yield after repeated for 8 times. In addition, a continuous flow reaction device was designed using the Pd/SiO_2 catalyst to effectively improve the production efficiency of biphenyl.

Graphic Abstract

Pd/SiO_2 catalyst constructed with the strategy of strong electrostatic adsorption (SEA) possesses uniformly dispersed and highly exposed Pd sites which can be easily transformed into electron-deficient $Pd^{\delta+}$ and strengthened stability for itself due

Xizheng Fan and Jingyi Yang have equally contributed to the work.

Electronic supplementary material The online version of this article (https://doi.org/10.1007/s10562-020-03465-9) contains supplementary material, which is available to authorized users.

Extended author information available on the last page of the article

Published online: 02 January 2021

to its strong interaction with the front surface of the carrier, and has been endowed the outstanding catalytic performance for Suzuki−Miyaura cross-coupling reaction.

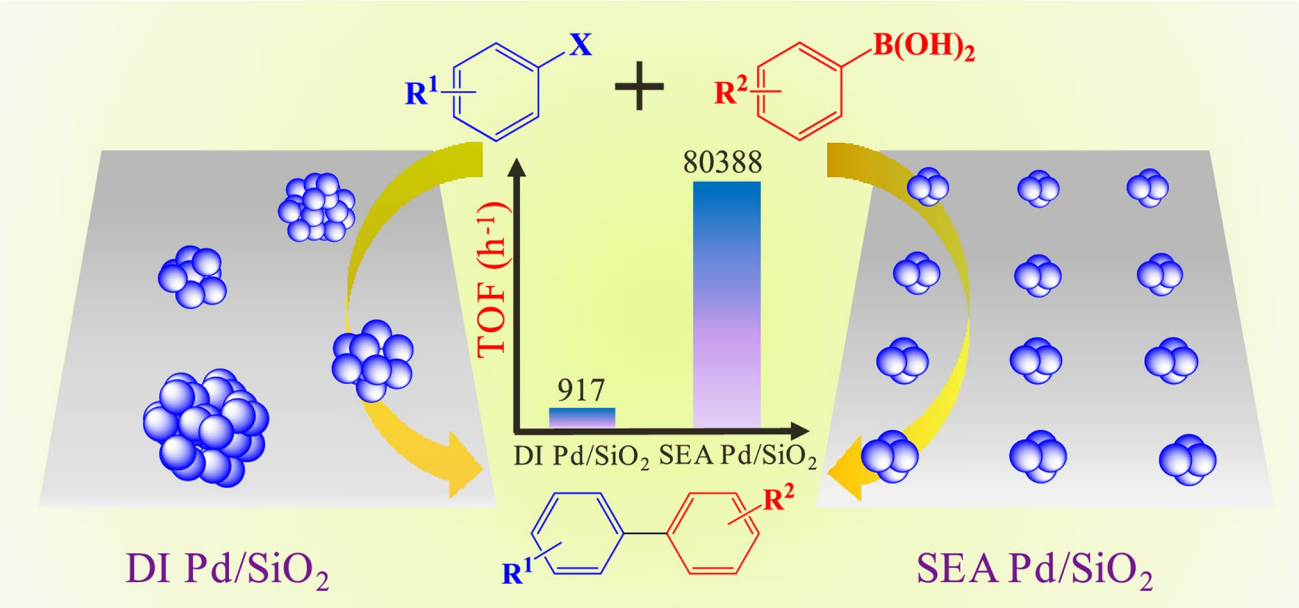

Keywords Pd/SiO_2 · Heterogeneous catalyst · Strong electrostatic adsorption · Suzuki–miyaura

1 Introduction

The formation of carbon–carbon bonds is fundamentally important reaction of synthetic organic chemistry, due to the widespread bonds in lots of natural products, pharmaceuticals, bio-active molecules and advanced materials. Among the array of methods developed over the years, Suzuki–Miyaura cross-coupling reactions have been documented as the straightforward and efficient approach for the preparation of carbon–carbon bonds, with mild conditions, satisfactory selectivity, facile operation and extensive tolerance of functional groups [1–6]. Therefore, Suzuki–Miyaura cross-coupling reactions have occupied more special position based upon its versatility, compatibility and key contributions to various disciplines including organic compounds synthesis, materials science and drug synthesis, which is publicly recognized for the effect to the rapid development in the field of chemical synthesis [7–9].

The variety and activity of metal catalysts are the main factors for Suzuki–Miyaura cross-coupling reactions. Palladium as a high-efficiency catalyst can provide higher conversion constant, which can be regulated to improve its catalytic performance through the choice of ligands, surfactants or carriers [10–15]. As the development of robust heterogeneous catalysts, multitudinous efforts have been focused on nano-composite containing Pd to obtain the development of more satisfactory performance [16, 17]. Obviously, the size and dispersion of the supported Pd nanoparticles (Pd NPs) are the primary factors affecting the activity, which have been well documented by references [18, 19]. However, Pd clusters having high surface energy, are prone to agglomeration with poor stability. It's difficult to carry out size-controlled synthesis for the particles on the surface of the support. In general, the solution to such methods is mainly to use surfactants, organic ligands and grafting on the carrier during the preparation process, increasing costs and difficulties and the risk of polluting the environment [20]. Therefore, an imperious demand has emerged for new strategy that can manufacture highly active Pd catalyst which can provide enjoyable results in the green solvent system by using benign chemical additives, and is easily recycled and cost-effective.

The Regalbuto etc. has developed the strong electrostatic adsorption (SEA) method (oxide surfaces become protonated or deprotonated to adsorb such anions or cations) which brings the uplifting news for the preparation of highly active heterogeneous nano-catalysts [21–24]. Compared with the methods of traditional wet impregnation or equal volume impregnation, the convenient and low-cost SEA strategy can effectively solve the disadvantages of large average size and wide size distribution without any explicit surface functionalization and capping agents. So we prepared palladium-loaded silica catalyst (Pd/SiO_2) including the superfine size (about 1.3 nm average value) and uniform

dispersion of Pd by SEA method. It is employed as catalyst for Suzuki–Miyaura reaction, which can afford excellent catalytic activity with highlighted advantages of structural, to remarkably improve to 99.5% yield adding 0.05 mmol% catalyst in the mild conditions. And it can be reused up 8 times with the robust catalytic performance, and further promoted to practical application field.

2 Experimental Section

2.1 Chemicals

Aladdin Aerosil 300 (hydrophilic type, BET SA-300 m^2/g, Point zero charge = 4.2) was used as the support of catalysts. Tetraamminepalladium (II) chloride monohydrate ($Pd(NH_3)_4Cl_2$, Pd ≥ 41%, Adamas-beta) was used as the cationic precursor salt for the catalyst preparation. The substrates (all are more than 99.00% pure) of Suzuki–Miyaura cross-coupling reaction including aryl halides (TCI and McLean), 2-bromine naphthalene (McLean), areneboronic acids (TCI and McLean), etc., were directly used after purchase without further purification. Base reagents contained sodium carbonate (Na_2CO_3, Sinopharm), potassium carbonate (K_2CO_3, Sinopharm), cesium carbonate (Cs_2CO_3, McLean), sodium bicarbonate ($NaHCO_3$, Sinopharm), sodium hydroxide (NaOH, Sinopharm), potassium hydroxide (KOH, Sinopharm), ammonia (NH_4OH, McLean), sodium acetate ($CH_3COONa.3H_2O$), disodium hydrogen phosphate ($Na_2HPO_4{\cdot}7H_2O$), urea (CON_2H_4, McLean); were analytically pure. Ethanol (Aladdin, 99.90%) and deionized water were used as the reaction solvent, and ethyl acetate (Aladdin, 99.99%) was as an extractant. The whole experiment was done with deionized water. The same metal precursor and silica support were used for catalysts prepared by the methods of strong electrostatic adsorption (SEA) and dry impregnation (DI).

2.2 S-Pd_X/SiO_2 Synthesis by SEA

SEA catalyst was prepared by controlling the pH relative to the surface point of zero charge (PZC) which decided what kind of precursors to be used. The convenient and reliable synthesis process for the Pd/SiO_2 catalysts are exhibited in Scheme 1 [22], and briefly described as follows. Tetraammine palladium chloride (1.26 g) as precursor, was dissolved in 1000 mL of deionized water under the ambient temperature for the whole operation. Based on the theoretical loading of Pd species, the 9.70 mL above solution and 290.30 mL deionized water were added into a 500 mL beaker. Then the pH of the precursor solutions was adjusted to 11.5 using ammonium hydroxide. 1.0 g silica was dispersed into the above liquid phase, then rapidly magnetic stirring for 1.0 h at room temperature to obtain the homogeneous white gelatum. During this period, the pH of above system was measured with a pH meter every 10 min, and ensured that the pH was maintained at 11.5 by continuously adding ammonium hydroxide. Then, the gelatum was centrifuged and washed three times with deionized water to remove redundant ammonium hydroxide. And the collected precipitate was dried in a vacuum oven at 60 °C to get the bulk named $Pd^{2+}{}_{0.8}/SiO_2$. The $Pd^{2+}{}_{0.8}/SiO_2$ ground

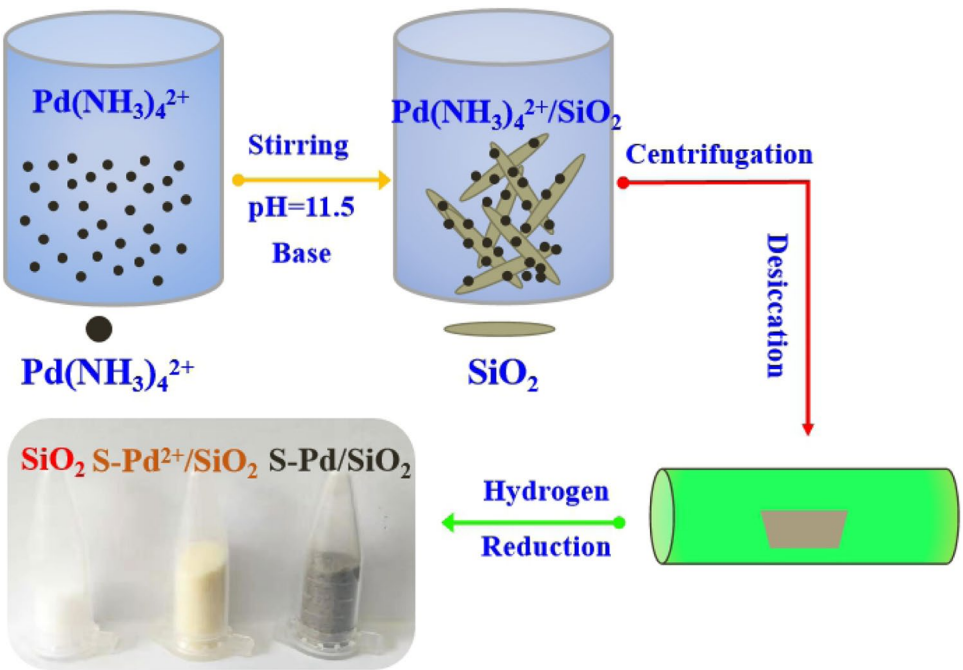

Scheme 1 Illustration of Pd catalyst assembled on the surface of SiO_2

into powder was calcined in muff furnace at 120 °C for 4 h. Immediately, the sample was placed in a tube furnace with the controllable temperature, reduced at 400 °C for 2 h in the atmosphere of H_2/N_2 mixture gas (10 vol% in H_2) and collected, which was named the S-$Pd_{0.8}/SiO_2$ catalyst with 0.8 wt% Pd. The synthesis of S-Pd_X/SiO_2 catalysts with different Pd quality content followed the same process (X is the theoretical loading of Pd).

2.3 D-$Pd_{0.8}/SiO_2$ Synthesis by DI

Meanwhile, we also prepared the D-Pd/SiO_2 with the uniform chemicals and weight load as the SEA sample (S-$Pd_{0.8}/SiO_2$) by the procedure of dry impregnation [25, 26]. Pore volume of the silica was determined to be 2.4 mL/g. So the 0.02 g of $Pd(NH_3)_4Cl_2$ was dissolved in 2.4 mL of deionized water for 1.0 g DI catalyst. The support and 2.4 mL precursor solution were added into a centrifuge tube, and the mixture slurry was shaken and churned to ensure complete wetting the silica with the solution. And the remaining formula was undifferentiated with the synthesis of S-$Pd_{0.8}/SiO_2$ to manufacture the D-$Pd_{0.8}/SiO_2$.

2.4 Characterizations

The morphology and structure of the material were obtained by the following methods. The crystal structures of the catalysts were determined by X-ray powder diffraction (XRD) on a D8ADVANCE in the range of 10 ~ 80°. The morphology of the samples was observed using the high resolution transmission electron microscopy (HR-TEM) on a FEI TalosF200S operating at an acceleration voltage of 200 kV, and high angle annular dark field-scanning transmission elec-tron microscopy (HAADF-STEM) on a spherical aberration correction electron microscope (Titan Cubed Themis G2 300). X-ray photoelectron spectroscopy (XPS) measurement was performed with a Thermo Scientific-ESCALAB 250XI multifunctional imaging electron spectrometer to research the valence states of metal. Brunauer–Emmett–Teller (BET) data of catalysts degassed at 120 °C for 6 h, were obtained by nitrogen sorption experiments conducted at 77 K using the Quantachrome Autosorb Gas Sorption analyzer. The UV spectra were scanned with Shimadzu UV-2450 UV–Visible spectrophotometer at wavelength of 240 ~ 800 nm with a speed of 0.5 nm/s. The metal loadings was determined by EDX spot scanning on the */Zeiss/Auriga FIB SEM. Infrared spectroscopy experiments were performed on a Bruker Vertex 70 V vacuum Fourier infrared spectrometer with the test conditions: hydrogen reduction at 400 °C for half an hour, nitrogen purge for half an hour to cool down, CO adsorption at room temperature until saturated adsorption, nitrogen purge at room temperature until the free gas phase CO was desorbed clean. H_2-TPR (temperature programmed reduction of hydrogen) of metal oxides was confirmed on the Quanrachrome Autosorb-IQ gas adsorption analyzer attached to a Pfeiffer Vacuum QME220 mass spectrometer. The dispersion of metallic Pd was detected by CO pulse chemisorption with 100 mg weighed sample (~ 100 mg), which was calculated with the assumptions of Pd and CO (stoichiometry of 1:1).

2.5 Evaluation of Catalysts for Suzuki–Miyaura Coupling Reaction

A typical probe of Suzuki–Miyaura cross-coupling reaction, used to evaluate the catalytic activity of the catalysts, was that bromobenzene (1.0 mmol) and phenylboronic acid (1.5 mmol) as the substrates were dissolved in the mixed liquor of ethanol (5 mL) and water (5 mL) containing base (1.5 mmol) and Pd/SiO_2 catalyst (0.5 mmol‰). The reaction was taken place in a flask under a mild environment. After removing the excess phenylboric acid by sodium hydroxide, the products were obtained through extraction procedure using ethyl acetate. Finally, the final yield of target product was determined by the gas chromatograph. Bromobenzene could be replaced by aryl halides with a variety of substituents and bremnaphthalene, and phenylboronic acid was also replaced by areneboronic acids containing the para substituent groups.

2.6 Recyclability and Stability of Catalysts

The stability of the catalyst was identified by the representative reaction of bromobenzene and phenylboronic acid as the substrates. The recycle of catalyst was achieved through the following procedures: (i) Product was separated from the reaction system by extracting with 0.02 mol/L sodium hydroxide and ethyl acetate. (ii) The catalyst was gathered by centrifugation, and washed three times by sodium hydroxide solution and ethanol to remove the absorbed substrate. (iii) The collected solid was dispersed in a little amount of ethanol and reused for the next run.

In addition, a continuous flow reaction was performed, which was simply described as follows. The reactor was placed in a controlled temperature water bath, where a well-proportioned solvent was added to disperse a certain amount of catalyst. The substrates and base (1.5 equiv. of bromobenzene) were dissolved in the prepared solvent and stirred continuously. The mixture was transported to the bottom of the reactor by a constant flux pump with adjustable flow rate and pressure. Under constant pressure, the mixture after reacting was squeezed from the top of the reaction solution and collected in a conical flask. Finally, the product was obtained by extraction, separation and purification. In order to ensure the product does not precipitate from the reaction

liquid and does not affect the reaction, we use the solvent of water and ethanol (volume ratio = 1/4).

3 Results and Discussion

3.1 Structural Investigations

The catalyst prepared by controlling dry impregnation (DI) with 0.8 wt% Pd (D-$Pd_{0.8}/SiO_2$) contains three representative peaks of Pd at 40.1°, 46.6° and 68.1° in the XRD pattern (Fig. 1a), corresponding to the primary diffraction of (111), (200) and (220). It can be further confirmed that the irregular face-core cube for Pd is larger with average size of 9.8 nm (Fig. S1) [27]. Amazingly, to the catalyst prepared by SEA with 0.8 wt% Pd (S-$Pd_{0.8}/SiO_2$), obvious peaks do not appear in the result of XRD, because of containing the smaller Pd NPs which can be observed directly from Fig. 1b, d, and have an average of 1.3 nm from the distribution histogram in Fig. 1c [28, 29]. The uniform dispersion of Pd species is also demonstrated by the elemental distribution test results of the

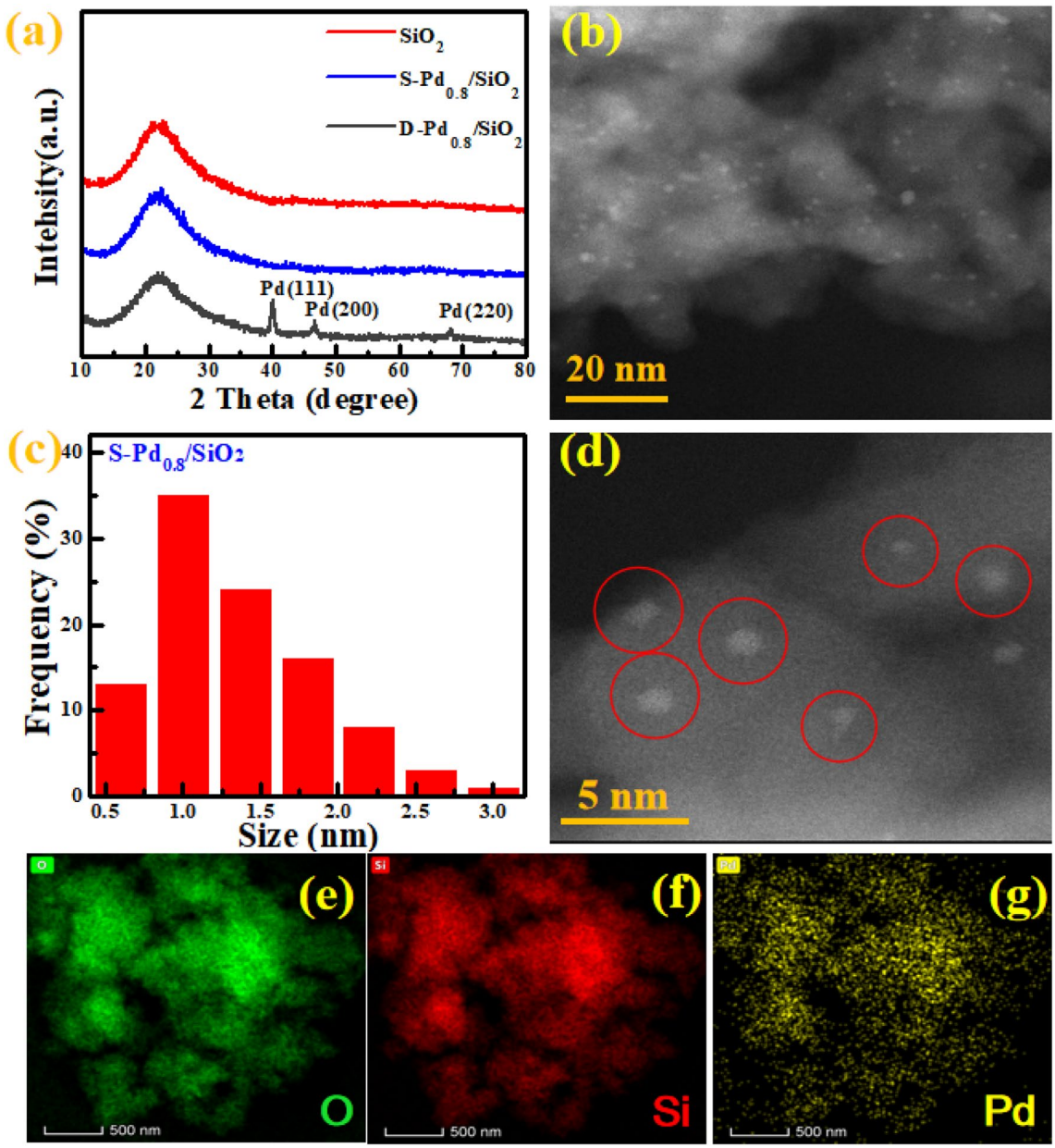

Fig. 1 Morphology and structure analysis of the Pd/SiO_2 samples: **a** XRD patterns of SiO_2, S-$Pd_{0.8}/SiO_2$ and D-$Pd_{0.8}/SiO_2$; **b** HADDF-STEM, **c** particle size distribution histogram, **d** AC-STEM and (e ~ g) EDX mapping images of S-$Pd_{0.8}/SiO_2$

catalyst through the mapping diagram (Fig. 1e ~ g). Furthermore, the EDX result in Fig. S2 testifies that 0.78 wt% Pd content of S-$Pd_{0.8}/SiO_2$ is consistent with the theoretical load. The as-prepared catalysts by SEA with different Pd content (S-Pd_X/SiO_2) have same phenomenon and possess uniformly dispersed and weeny particles, which were observed from results of XRD patterns (Fig. S3A) and HADDF-STEM (Fig. S3B). Besides, the dispersion of Pd NPs on the surface of $Pd_{0.8}/SiO_2$ calculated by CO pulse chemisorption is 43%, which is fourfold that of D-$Pd_{0.8}/SiO_2$ (9.7%), due to the ultrafine NPs and excellent dispersion to provide more active sites for the adsorption of CO [30]. The above results obviously prove that Pd catalysts prepared by SEA have the great structural advantage over the catalyst of DI.

X-ray photoelectron spectroscopy (XPS), has been employed to analyze Pd 3d and O 1 s of S-$Pd_{0.8}/SiO_2$ (Fig. 2a, b, S4). The peak of Pd^0 has been significantly deviated from the standard metallic Pd (335.2 eV) to higher binding energy (336.2 eV), which can be proofed by the result of Pd^0 3d for S-$Pd_{0.8}/SiO_2$ [31]. Meanwhile, the binding energy of O 1 s has the shift to lower binding energy, which is from 530.6 eV to 530.3 eV, because that O tends to get electrons from Pd species [32]. Hence, it implies that there is close interaction between the Pd atoms with the O atoms in the surface of silica. Unsurprisingly, the peak of Pd and O species in D-Pd0.8/SiO2 does not give significant change.

TPR profile demonstrates that the D-$Pd_{0.8}/SiO_2$ exhibits a low reduction temperature of ~ 150 °C, but the SEA sample requires a higher temperature of ~ 348 °C for Pd reduction, which also verifies that the Pd atoms have the much stronger interaction with the silica support (Fig. 2c), implying the Pd NPs of S-$Pd_{0.8}/SiO_2$ have better stability in the reacting system with stronger support interaction in common with XPS.

Infrared (IR) spectroscopy with CO as a probe molecule (Fig. 2d) shows that the S-$Pd_{0.8}/SiO_2$ has the obvious absorption peaks, which are labeled as bridge CO peak at 1948 cm^{-1} and line CO peak at 2087 cm^{-1} [33, 34]. Compared with the D-$Pd_{0.8}/SiO_2$, the peak value is significantly stronger to demonstrate that S-$Pd_{0.8}/SiO_2$ has more adsorption sites to suggest that the surface of silica is Pd-rich. In contrast, the weakly infrared peak for D-$Pd_{0.8}/SiO_2$ at 1981 cm^{-1} corresponding the Pd specie with contiguous dual sites for CO absorption, which is closely related to the larger Pd NPs resulting in the fewer number of Pd atoms exposed on the surface in per unit mass [35, 36].

Comparing the UV–Vis spectrogram of Pd^{2+} in S-Pd^{2+}/SiO_2 and D-Pd^{2+}/SiO_2 in Fig. 3a, the inconsistent absorption peak is at 351 nm and 399 nm (the normal Pd ions absorption peak at 410 nm) for S-Pd^{2+}/SiO_2 and D-Pd^{2+}/SiO_2, respectively [37]. This indicates that Pd atoms in

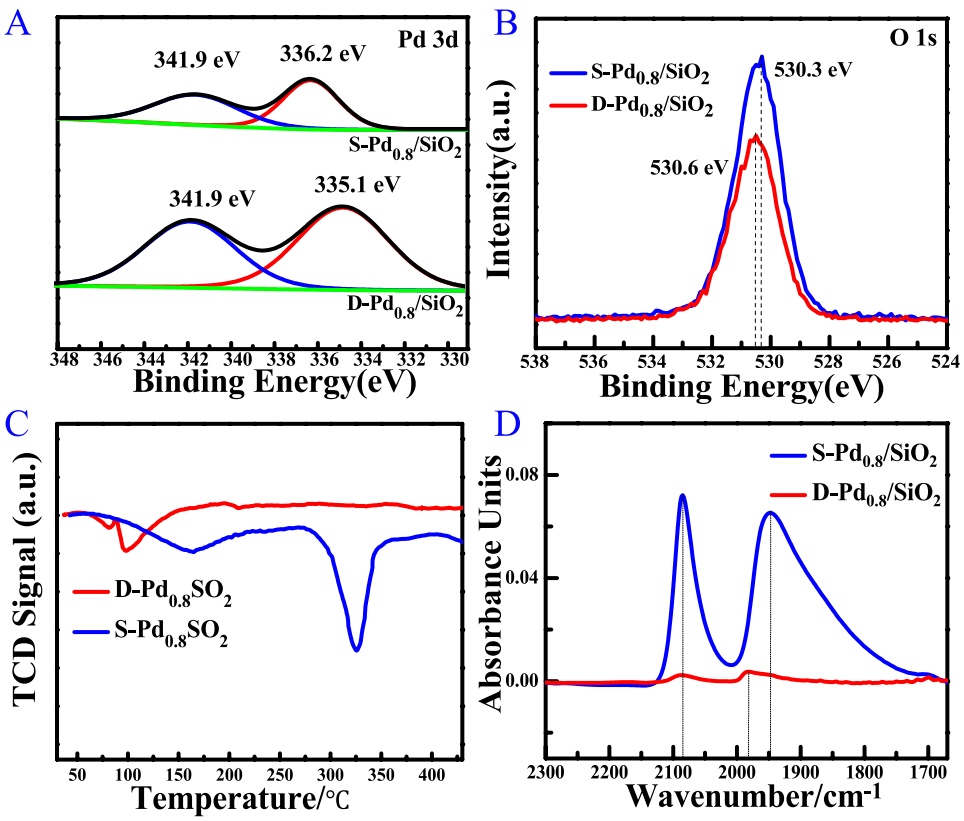

Fig. 2 XPS spectra of **a** Pd 3d, **b** O 1 s, **c** TPR and **d** CO in-situ IR of $Pd_{0.8}/SiO_2$ preparation by SEA and DI, respectively

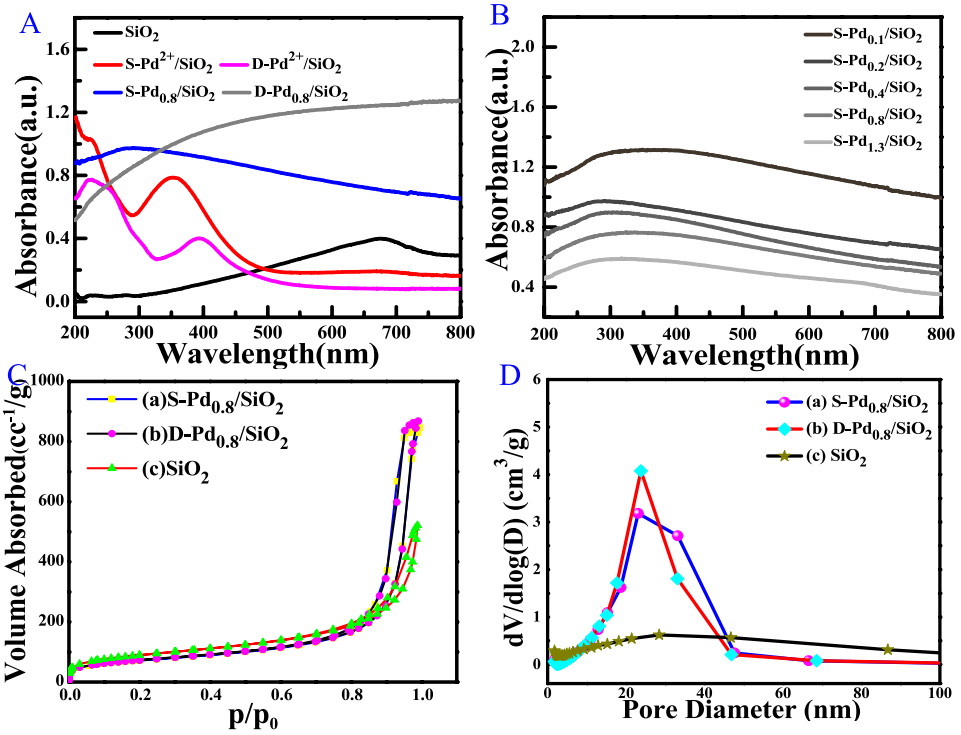

Fig. 3 UV–Vis spectroscopic images of **a** SiO_2; Pd^{2+}/SiO_2 and Pd/SiO_2 prepared by SEA and DI, **b** $S\text{-}Pd_X/SiO_2$(X = 0.1, 0.2, 0.4, 0.8, 1.3) with different content of Pd, **c** N_2 adsorption–desorption isotherms and **d** Pore size distribution calculated by the BJH method with Physical adsorption apparatus for SiO_2, $S\text{-}Pd_{0.8}/SiO_2$, $D\text{-}Pd_{0.8}/SiO_2$

$S\text{-}Pd^{2+}/SiO_2$ have a stronger interaction with superficial O and cause the absorption peak to have the conspicuous blue shift. The absorption intensity of $S\text{-}Pd_{0.8}/SiO_2$ in infrared and visible regions is significantly lower than that of $D\text{-}Pd_{0.8}/SiO_2$, but opposite in ultraviolet region, which can be affirmed by showing plasmon band at around 300 nm for the ultrafine Pd particles [38]. All $S\text{-}Pd_X/SiO_2$ samples with different Pd content also have such performance (Fig. 3b), and as the content of Pd increased, the color of appearance for samples gradually deepen.

The information of the pore structure from N_2 adsorption–desorption isotherms illustrates that the amorphous silica is the typical mesoporous material (Fig. 3c and d) [39, 40]. The pore structure parameters in Table S1 show that the surface area of $S\text{-}Pd_{0.8}/SiO_2$ and $D\text{-}Pd_{0.8}/SiO_2$ have suffered from a decline compared with SiO_2, and the reduction are more remarkable for $D\text{-}Pd_{0.8}/SiO_2$, because of the alkali etching and the adsorption of Pd NPs.

The characterization results fully confirm that the ultrafine Pd NPs prepared by SEA benefit from the strong interaction between the electron-rich O element on the carrier and the electron-deficient Pd complex under the alkaline atmosphere, which can reduce the surface forces between the Pd NPs. However, due to the poor binding force between the carrier and Pd species and the high surface energy, the Pd NPs of DI catalyst can continuously grow larger with the adjacent Pd particles by dry impregnation method.

3.2 Catalytic Activities of Pd/SiO_2 in Suzuki–Miyaura Reactions

To examine the activity of the as-prepared catalysts for Suzuki–Miyaura, the model reaction of benzeneboric acid and bromobenzene was selected for the optimization of the reaction conditions. As shown in Fig. 4, Fig. S5 and Table S2, S3, large variations for the reactivity were observed depending on the catalyst, time, temperature, base and solvent, used in the reactions [41–43]. As summarized, it was found that the following conditions as the standard reaction conditions: bromobenzene (1.0 eq.), phenylboronic (1.3 eq.), $S\text{-}Pd_{0.8}/SiO_2$ (0.05 mmol %), KOH (1.5 eq.), H_2O/EtOH (volume ratio is equal to 1:1) as the solvent. Biphenyl was synthesized with up to > 99% yield, at 40 °C for 30 min. As shown in the Fig. 4A and Fig. 4B, the catalytic performance of the $S\text{-}Pd_{0.8}/SiO_2$ was significantly better comparing with $D\text{-}Pd_{0.8}/SiO_2$. Specific result was that $D\text{-}Pd_{0.8}/SiO_2$ has 22.9% yield in 40 °C for 30 min to be ascertained poorer performance. In addition, a more intuitive result in Fig. 4c was expressed by TOF values calculated at a conversion rate of ≤ 50%. The conversion frequency of the $S\text{-}Pd_{0.8}/SiO_2$ (80,388 h^{-1}) was around 87 time for the $D\text{-}Pd_{0.8}/SiO_2$ (917 h^{-1}) and 34 time for commercial Pd/C (2288 h^{-1}) under the same conditions. As shown in Table S4, the significantly high TOF (even reaching 10^5 h^{-1} at 60 °C) was given using the SEA catalysts with different Pd loads under different temperatures. Furthermore, the expansion of substrates for

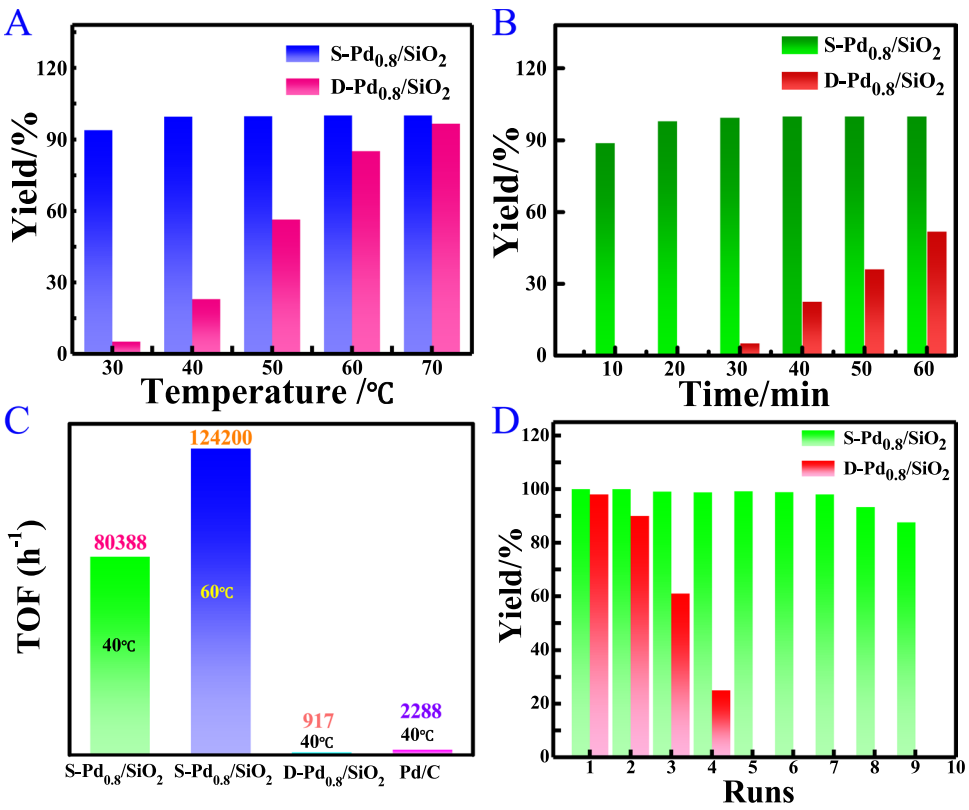

Fig. 4 Investigation of the factors influencing the Suzuki–Miyaura coupling reactions, including **a** temperature and **b** time, **c** comparison for TOF values of S-$Pd_{0.8}/SiO_2$, D-$Pd_{0.8}/SiO_2$ and commercial 10 wt% Pd/C, **d** cyclic properties of S-$Pd_{0.8}/SiO_2$ and D-$Pd_{0.8}/SiO_2$

Suzuki–Miyaura coupling reactions had been carried out at the best experimental conditions. A series of aryl halides and boronic acids were tested. As summarized in Table 1 and Table S5, the S-$Pd_{0.8}/SiO_2$ catalyst exhibited highly activity for the different substrates with varieties of functional groups, giving the corresponding products with higher yields in mild conditions. High dispersion and ultrafine size of Pd NPs afforded more reactive sites to increase the interacting chance for substrates with the nano-metal and made contributions to improving catalyst activity. When the substrates and catalyst were simultaneously expanded by a factor of 10, the yield was still 99% (Table 1, Entry 19).

To illustrate the superiority of the as-prepared Pd/SiO_2 by the SEA strategy, a comparison was made between S-$Pd_{0.8}/SiO_2$ with the recently reported Pd nano-catalysts. As shown in Table S6, the S-$Pd_{0.8}/SiO_2$ catalyst synthesized preferably gave the excellent yield with the short reaction time, secure solvent, as well as low temperature. This fully demonstrates that S-Pd/SiO_2 catalyst is one of the best classes of heterogeneous catalysts, affording the highest yield with the lower catalyst loading of 0.05 mmol% under the mild environment.

Importantly, industrial production of chemicals is of great significance to value maximization. According to the constant pressure principle of the reaction vessel, we designed a facile continuous production device (as shown in Fig. S6) to ensure that the reactant feed was in an equilibrium state with reaction mixture discharge, improving the reaction volume and production efficiency. And the process of reaction could be controlled by the feed flow and the thermostat. The production results were shown in Entry 20, 21 of Table 1, which still gave the satisfactory yield more than 90% according to 30 mL/h flow rate at 40 ~ 60 °C.

3.3 Recyclability of Catalyst

To determine the cycling performance and stability of catalysts, which were the highly important indicators for catalyst quality, the cyclic experiment was carried out. As shown in Fig. 4d, the S-$Pd_{0.8}/SiO_2$ could be circulated more than 8 times, which still maintained the yield of more than 90%. On the contrary, the D-$Pd_{0.8}/SiO_2$ did not exhibit catalytic activity again after nearly 4 cycles. The amorphous structure of silica is damaged to some extent after the catalytic reaction for the carrier silica because of its slightly worse alkali tolerance and there is a certain degree of agglomeration of nano-palladium to increase the size of nano-particles (Fig. 5a), which is the main reason for the reduction of activity. Meanwhile, the catalyst still containing a large number of fine Pd NPs with particle size less than 3 nm, does not increase the diffraction property of palladium to X-ray (Fig. 5b). In addition, the hot filtration experiment for S-$Pd_{0.8}/SiO_2$ was performed to check Pd-leaching behavior. The result testified that the filtrate from the S-$Pd_{0.8}/SiO_2$ catalyst did not given the detectable conversion of biphenyl products.

Table 1 Suzuki–Miyaura cross-coupling reactions of various Ar-X and Ar-$B(OH)_2$ catalyzed by S-Pd/SiO_2[a]

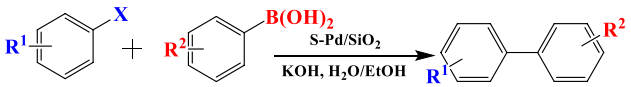

Entry	R^1	X	R^2	t/min	T/°C	Yield[b] (%)
1	H	Br	H	30	40	> 99.5
2	4-$COCH_3$	Br	H	30	40	> 99.5
3	4-CN	Br	H	30	40	97
4	4-CHO	Br	H	60	60	99
5	4-OCH_3	Br	H	30	40	99
6	4-OCH_3	I	H	30	40	99
7	4-CH_3	Br	H	30	40	> 99.5
8	H	Br	4-F	30	40	99
9	H	Br	4-CH_3	30	40	> 99.5
10	H	Br	4-$COCH_3$	30	40	98
11	4-OH	I	H	60	60	97
12	4-OH	Br	H	60	60	95
13	4-$COCH_3$	Br	4-F	30	40	99
14	4-$COCH_3$	Br	4-CH_3	30	40	99
15	4-$COCH_3$	Br	4-$COCH_3$	30	40	96
16	4-CH_3	Br	4-F	30	40	98
17	4-CH_3	Br	4-CH_3	30	40	99
18	4-CH_3	Br	4-$COCH_3$	30	40	95
19[c]	H	Br	H	30	40	99
20[d]	H	Br	H	/	40	90
21[d]	H	Br	H	/	60	97

[a]Reaction conditions: Ar-X (1.0 mmol), Ar-$B(OH)_2$ (1.3 mmol), KOH (1.5 mmol), S-$Pd_{0.8}/SiO_2$ (0.05 mmol% Pd), H_2O/EtOH (5 mL + 5 mL)

[b]Yields were determined by GC

[c]The substrates and catalyst were expanded by a factor of 10

[d]The reaction result of the flow are obtained under 30 mL/h flow rate with 0.5 mmol% catalyst. The ratio of H_2O/EtOH is 1/4

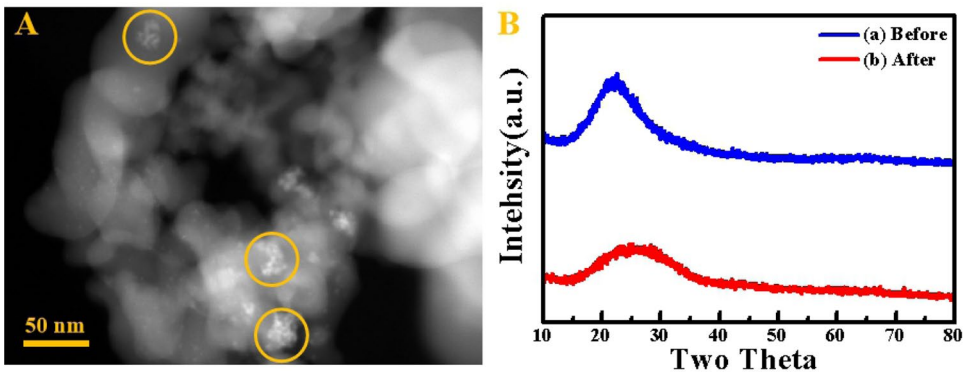

Fig. 5 **a** HAADF-STEM image of the S-$Pd_{0.8}/SiO_2$ catalyst after 8th cycle; **b** XRD patterns of the S-$Pd_{0.8}/SiO_2$ catalyst before and after 8th cycle

4 Conclusions

In summary, the practical and efficient approach for the synthesis of various biphenyl compounds has been developed based on S-Pd/SiO_2-catalyzed Suzuki–Miyaura reactions with respect to aryl halides and areneboronic acids under the mild conditions. The versatile SEA strategy has determined that the S-Pd/SiO_2 catalyst as a high-performance, inexpensive and easily recyclable nano-materials, shows the substantial improvement in this kind reactions, due to high dispersion and ultrafine

nanoparticles of Pd species. This work develops the new possibilities for constructing the high-efficiency heterogeneous Pd-based catalyst without any ligands and capping reagents, which has great potential and superiority for industrial production because of the remarkable activity and cycling stability.

Acknowledgments This research was supported by the National Natural Science Foundation of China (Grant nos. 21403053, 21502175 and U1404503), Dalian Institute of Chemical Physics (N-19-11), Key Laboratory of Henan Province Drug Quality Control and Evaluation.

Compliance with Ethical Standards

Conflict of interest The authors declare that they have no confict of interest.

Appendix A. Supplementary material

Supplementary data to this article can be found online which contains TEM images, XRD pattern, EDX, fitting results of XPS spectra and XPS, tables and figures of experimental datum, literature data for comparison, and schematic diagram of flow device.

References

1. Fihri A, Bouhrara M, Nekoueishahraki B, Basset JM, Polshettiwar V (2011) Chem Soc Rev 40:5181–5203
2. Zhou D, Tan XY, Wu HM, Tian LH, Li M (2019) Angew Chem Int Ed 58:1376–1381
3. Lei P, Meng GR, Ling Y, An J, Szostak M (2017) J Org Chem 82:6638–6646
4. Chen X, Engle KM, Wang DH, Yu JQ (2009) Angew Chem Int Ed 48:5094–5115
5. He J, Wasa M, Chan KSL, Shao Q, Yu JQ (2017) Chem Rev 117:8754–8786
6. Yang Y, Lan J, You J (2017) Chem Rev 117:8787–8863
7. Iwai T, Konishi S, Miyazaki T, Kawamorita S, Yokokawa N, Ohmiya H, Sawamura M (2015) ACS Catal 5:7254–7264
8. Ejlersen M, Lou CG, Sanghvi YS, Tor Y, Wengel J (2018) Chem Commun 54:8003–8006
9. Shen D, Xu YJ, Shi SL (2019) J Am Chem Soc 141:14938–14945
10. Fernández E, Rivero-Crespo MA, Domínguez I, Rubio-Marqués P, Oliver-Meseguer J, Liu LC, Cabrero-Antonino M, Gavara R, Hernández-Garrido JC, Boronat M, Leyva-Pérez A, Corma A (2019) J Am Chem Soc 141:1928–1940
11. Dhakshinamoorthy A, Asiric AM, Garcia H (2015) Chem Soc Rev 44:1922–1947
12. Ding SY, Gao J, Wang Q, Zhang Y, Song WG, Su CY, Wang W (2011) J Am Chem Soc 133:19816–19822
13. Rajabzadeh M, Khalifeh R, Eshghi H, Bakavoli M (2018) J Catal 360:261–269
14. Yin Z, Lin L, Ma D (2014) Catal Sci Technol 4:4116–4128
15. Huang F, Deng Y, Chen Y, Cai X, Peng M, Jia Z, Ren P, Xiao D, Wen X, Wang N, Liu H, Ma D (2018) J Am Chem Soc 140:13142–13146
16. Hamdi J, Blanco AA, Diehl B, Wiley JB, Trudell ML (2019) Org Lett 21:213471–213475
17. Arpad M (2011) Chem Rev 111:2251–2320
18. Handa S, Wang Y, Gallou F, Lipshutz BH (2015) Science 349:1087–1091
19. Siamaki AR, Lin Y, Woodberry K, Connellc JW, Gupton BF (2013) J Mater Chem A 1:12909–12918
20. Chen ZP, Vorobyeva E, Mitchell S, Fako E, Ortuño MA, López N, Collins SM, Midgley PA, Richard S, Vilé G (2018) Pérez-Ramírez. J Nat Nanotechnol 13:702–707
21. Wong A, Liu Q, Griffin S, Nicholls A, Regalbuto JR (2017) Science 358:1427–1430
22. Jiao L, Regalbuto JR (2008) J Catal 260:329–341
23. Lambert S, Job N, D'Souza L, Pereira MFR, Pirard R, Heinrich B, Figueiredo JL, Pirard JP, Regalbuto JR (2009) J Catal 261:23–33
24. Spieker WA, Regalbuto JR (2001) Chem Eng Sci 56:3491–3504
25. Cao C, Yang G, Dubaud L, Maillardd F, Lamberta SD, Pirarda JP, Joba N (2014) Appl Catal B: Environ 150–151:101–106
26. Papadopoulou C, Vakros J, Matralis HK, Voyiatzis GA, Kordulis CJ (2004) Colloid Interface Sci 274:159–166
27. Liu Y, Bai XF, Li S (2018) Micropor Mesopor Mater 260:40–44
28. Samad JE, Hoenig S, Regalbuto JR (2015) ChemCatChem 7:3460–3463
29. Banerjee R, Liu QL, Tengco JMM, Regalbuto JR (2017) Catal Lett 147:1754–1764
30. Lupescu JA, Schwank JW, Fisher GB, Hangas J, Peczonczyk SL, Paxton WA (2018) Appl Catal B: Environ 223:76–90
31. Li JZ, Bai XF, Lv HF (2020) Ultrason Sonochem 60:104746
32. Dalby KN, Nesbitt HW (2007) Zakaznova-HerzogVP, King PL. Geochim Cosmochim Ac 71:4297–4313
33. Yang X, Li Q, Wang H, Huang J, Lin L, Wang W, Sun D, Su Y, Opiyo JB, Hong L, Wang Y, He N, Jia L (2010) J Nanopart Res 12:1589–1598
34. Ding KL, Cullen DA, Zhang LB, Cao Z, Roy AD, Ivanov IN, Cao DM (2018) Science 362:560–564
35. Chen MS, Cai Y, Yan Z, Gath KK, Axnanda S, Goodman DW (2007) Surf Sci 601:5326–5331
36. Hong R, He Y, Feng J, Li D (2017) AIChE J 63:3955–3965
37. Murata K, Eleeda E, Ohyama J, Yamamoto Y, Araid S, Satsuma A (2019) Phys Chem Chem Phys 21:18128–18137
38. Yee CK, Jordan R, Ulman A, White H, King A, Rafailovich M, Sokolov J (1999) J Langmuir 15:3486–3491
39. Naderi M (2015) Progress in Filtration and Separation. Academic Press, Massachusetts, pp 585–608
40. Thommes M, Kaneko K, Neimark AV, Olivier JP, Rodriguez-Reinoso F, Rouquero J, Sing KSW (2015) Pure Appl Chem 87:1051–1069
41. Dong Y, Jv JJ, Wu XW, Kan JL, Lin T, Dong YB (2019) Chem Commun 55:14414–14417
42. Hudson R, Katz JL (2018) ACS Sustainable Chem Eng 6:14880–14887
43. Feng J, Handa S, Gallou F, Lipshutz BH (2016) Angew Chem 128:9125–9129

Affiliations

Xizheng Fan[1] · Jingyi Yang[1] · Qingqing Pang[1] · Zhongyi Liu[1] · Panke Zhang[1] · Jing-He Yang[1,2]

✉ Panke Zhang
pkzhang@zzu.edu.cn

✉ Jing-He Yang
jhyang@zzu.edu.cn

[1] College of Chemistry, and Institute of Green Catalysis, Zhengzhou University, Zhengzhou 450001, People's Republic of China

[2] School of Chemical Engineering, Zhengzhou University, Zhengzhou 450001, People's Republic of China